Available online at www.sciencedirect.com
SCIENCE DIRECT®
Journal of Catalysis 231 (2005) 393–404
JOURNAL OF CATALYSIS
www.elsevier.com/locate/jcat

Stabilities of C_3–C_5 alkoxide species inside H-FER zeolite: a hybrid QM/MM study

Ville Nieminen [a], Marek Sierka [b], Dmitry Yu. Murzin [a], Joachim Sauer [b,*]

[a] *Laboratory of Industrial Chemistry, Process Chemistry Centre, Åbo Akademi University, FIN-20500 Turku/Åbo, Finland*
[b] *Institut für Chemie, Humboldt-Universität zu Berlin, Unter den Linden 6, D-10099 Berlin, Germany*

Received 9 November 2004; revised 28 January 2005; accepted 31 January 2005

Available online 23 March 2005

Abstract

Adsorption (π-complex formation) and chemisorption (alkoxide formation) of ethene, propene, 1-butene, and 1-pentene, as well as of isobutene and 2-methyl-1-butene, in zeolite H-FER are examined by a hybrid quantum mechanics/molecular mechanics (QM/MM) method that takes van der Waals (dispersion) interactions into account. The predicted heats of adsorption (36, 51, 45, 64, 41, 47 kJ/mol, respectively) fall into energy ranges inferred from experimental values for alkanes in H-zeolites. Vibrational frequencies are calculated for adsorbed butenes and butyl alkoxide species and compared with observed spectra for adsorbed 1-butene and isobutene. Primary and secondary alkoxide species are found to be significantly more stable than the adsorption complexes with chemisorption energies between 137 and 205 kJ/mol. The stability increases with the length of the alkyl chain. Geometrical constrictions close to the active site result in reduced stabilities of bulky alkoxide isomers. The *tert*-butyl and 1,1-dimethylpropyl species are less stable (chemisorption energies of 62 and 78 kJ/mol, respectively) or even nonexistent at sterically hindered framework positions. The implications of relatively stable alkoxide intermediates for hydrocarbon transformation reactions over H-zeolites are discussed.

Keywords: QM/MM hybrid method; Embedded cluster calculation; Zeolite; Ferrierite; Alkene; Adsorbtion; Alkoxide

1. Introduction

The proton forms of zeolites and zeolite-type materials are porous solid acids. They are used as catalysts for hydrocarbon transformation reactions, such as skeletal isomerization of linear butenes. The activity of these catalysts is based on the Brønsted acid function, that is, their ability to donate a proton to a hydrocarbon, which is transformed into a positively charged carbenium ion. This carbocation mechanism of acid-catalyzed organic reactions was originally formulated and developed for homogeneous catalysis in superacidic media and later used for heterogeneous catalysis by zeolites [1].

However, there is experimental and computational evidence that small protonated olefins do not exist as free carbenium ions, but rather as alkoxides bound to the aluminosilicate framework [1,2]. The carbenium ions of small hydrocarbons, such as butene, are transition structures [1]. Hence, reaction mechanisms have been suggested that assume alkoxides as intermediates. According to the monomolecular mechanism of butene isomerization [3,4], a 1-butene molecule adsorbs on the Brønsted acid site via the π-bond (see Fig. 1). Adsorption at O^aH is followed by protonation of the terminal $H_2C=$ carbon and formation of a σ-bond between the other $=CH-$ carbon and the O^b framework oxygen atom neighboring O^a. The alkoxide species formed undergoes skeletal isomerization through a cyclic transition state, yielding a primary alkoxide intermediate attached to O^a, which decomposes into adsorbed isobutene and a Brønsted site O^bH. A similar mechanism has been discussed for isomerization of 1-pentene (see Fig. 2 (Path b) of [5]). The monomolecular reaction mechanism has been widely accepted [6,7], but bimolecular mechanisms have also been suggested [8], and it is still controversial which mechanism

* Corresponding author.
E-mail address: js@chemie.hu-berlin.de (J. Sauer).

0021-9517/$ – see front matter
doi:10.1016/j.jcat.2005.01.035

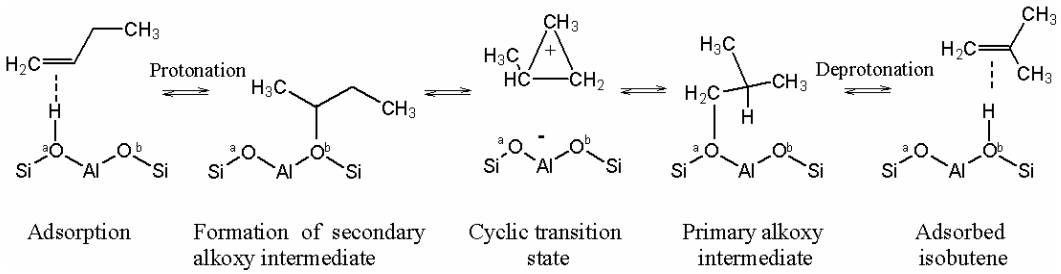

Fig. 1. Monomolecular reaction path of 1-butene skeletal isomerization.

is responsible for the high selectivity for isobutene [9,10]. Whether protonated olefins inside zeolites exist as alkoxides or as carbenium ion species and the possible role of these species as intermediates have been extensively debated in the literature [4,11–15].

In this work, we examine the relative stabilities of possible intermediates of the alkene isomerization in H-FER (proton form of ferrierite), that is, π-adsorption complexes of propene, butanes, and pentenes with the Brønsted sites and alkoxides formed on chemisorption of these alkenes. H-FER is an efficient catalyst for the skeletal isomerization of linear butenes, even applied commercially [6,8], and is therefore chosen as the zeolite catalyst for this study. There are several spectroscopic studies of the interaction of butenes with H-FER [16–18]. We use a hybrid quantum mechanics/molecular mechanics (QM/MM) embedded cluster method [19], which limits the QM description to the zeolite active site and the reacting hydrocarbon molecules. The remainder of the periodic zeolite structure and the interaction of the hydrocarbon with the zeolite framework are described by force fields. Compared with full periodic QM calculations, not only is the computational time significantly reduced, but, more importantly, more reliable adsorption energies are obtained [20,21] because the force field accounts for the (van der Waals) dispersion contributions, which dominate the hydrocarbon framework interactions. The QM-Pot approach used here [19] has been successfully applied to hydrocarbon reactions in H-zeolites before [20,21]. The QM-Pot method in particular [22,23] and the hybrid QM/MM approaches in general [24] have been reported to be very effective in describing interactions of reactants with active sites in heterogeneous catalysis. Previously adsorption of different butenes in H-FER [25,26] was studied by force fields only, with the use of the consistent force field [27] and its extension to zeolites [28,29].

2. Computational methodology

2.1. Hybrid QM/MM calculations on embedded clusters

In this study the hydrocarbon species inside the zeolite pore system are described by a hybrid quantum mechanics/molecular mechanics (QM/MM) embedded cluster method [19]. It treats the Brønsted acid site and the hydrocarbon by density functional theory (DFT) and the remainder of the periodic zeolite structure by a shell-model ion-pair potential. This potential function has been parameterized on DFT results for a variety of cluster models [30]. It takes the polarizability of the oxygen ions into account and yields zeolite structures and vibrational spectra in good agreement with the experiments [30]. The interaction of the hydrocarbon with the zeolite framework is described by force fields that include Lennard–Jones terms and point charge interactions. Compared with nonembedded cluster calculations, the QM/MM hybrid approach is more reliable since the effect of the periodic framework on the local geometry is taken into account. At the same time, compared with full DFT calculations on periodic structures, the computational effort is significantly reduced. For the particular problem of hydrocarbon reactions in zeolites, the hybrid QM/MM approach has the additional benefit that adsorption energies are described more accurately, because unlike DFT [31,32], force fields provide a good description of weak dispersion forces (van der Waals interactions) (see, e.g., [33] and references therein).

The hybrid QM/MM method defines the potential energy surface as

$$E(\text{System})_{\text{QM/MM}} = E(\text{System})_{\text{MM}} - E(\text{Cluster})_{\text{MM}} + E(\text{Cluster})_{\text{QM}}. \quad (1)$$

Here $E(\text{System})_{\text{QM/MM}}$ is the hybrid QM/MM energy of the whole periodic system. The MM energy of the whole system, $E(\text{System})_{\text{MM}}$, is corrected by addition of the QM result, $E(\text{Cluster})_{\text{QM}}$, for the cluster (active site + hydrocarbon) and subtraction of the corresponding MM result, $E(\text{Cluster})_{\text{MM}}$. Corresponding expressions exist for combined energy gradients and second derivatives, which ensure rotational and translational invariance [19].

Since the van der Waals interactions between the zeolite wall and the hydrocarbon are more reliably described by force fields than by current density functionals, the zeolite part of the embedded cluster is kept as small as possible. A model consisting of three tetrahedra, $(HO)_3SiOAl(OH)_2O Si(OH)_3$, is adopted. The dangling Si–O and Al–O bonds were saturated by H atoms with O–H bond distances of 96.66 and 96.28 pm for the SiO–H and AlO–H bonds, respectively. This raises the question of whether this cluster is large enough to properly describe reactive steps such as proton transfer to form carbenium ions or C–O bond formation to form alkoxides. When embedded in a shell-model ion-pair potential, the T3 cluster yields errors of less than 5 kJ/mol

for deprotonation energies and good approximations to full periodic DFT calculations for reactions for which the dispersion energy plays a minor role, as shown in [20,21].

The DFT calculations for the embedded cluster use the B3LYP functional [34–36] and the triple-zeta valence plus polarization (TZVP) basis set from the TURBOMOLE library [37]. The acidic form of the FER zeolite, H-FER, its deprotonated form, and all hydrocarbon species inside the FER zeolite were optimized with the QM-Pot program [19], which couples the TURBOMOLE program package [38–41] for the QM part (zeolite model + hydrocarbon) with the GULP program [42] for the force-field calculations on the full periodic zeolite structure. Second derivatives of the QM/MM energy with respect to the nuclear degrees of freedom were calculated for all of the structures to ensure that they are minima on the potential energy surface. The vibrational frequencies from the second derivatives (force constants) are scaled by a factor of 0.9614 [43] for better comparison with observed values. This scale factor accounts for both systematic errors with force constants and neglected anharmonicities. From the energies of adsorption, the heats of adsorption were calculated, which include zero-point vibrational energies, additional thermal contributions, and volume work. With the TZVP basis set the basis set superposition error is 4.3 and 5.9 kJ/mol for the π-adsorption complexes of 1-butene and isobutene on O^7H, respectively, (Table 3).

2.2. Thermodynamic functions from QM/MM calculations

To calculate thermodynamic functions we use molecular statistics within the harmonic oscillator–rigid rotor–ideal gas approximation as described in textbooks [44]. The energy of adsorption, ΔE_a, is obtained from the QM/MM energies of the adsorbate (a), the unloaded zeolite (ZOH) and the gas-phase alkene molecule (alkene)

$$\Delta E_a = E_a - E_{ZOH} - E_{alkene}. \quad (2)$$

The internal energy, U, and the entropy, S, of all three species are obtained from the (electronic) QM/MM energy, E, the zero-point vibrational energy, E_{ZPV}, and temperature-dependent contributions arising from the partition function q.

$$U = E + E_{ZPV} + RT^2\, \mathrm{d}\ln q/\mathrm{d}T, \quad (3)$$

$$S = R\ln q + RT\, \mathrm{d}\ln q/\mathrm{d}T. \quad (4)$$

For the gas-phase alkenes, q has rotational, translational, and vibrational contributions, $q_{alkene} = q_{rot}q_{trans}q_{vib}$, whereas the unloaded zeolite and the adsorbate are assumed to be rigid in space and have only vibrational degrees of freedom, $q_{ZOH/a} = q_{vib}$.

Use is made of the harmonic vibrational frequencies calculated by QM/MM to evaluate q_{vib}. The standard enthalpy of adsorption is obtained as

$$\Delta H_a = \Delta U_a - RT, \quad (5)$$

where RT arises from the volume work pV.

The Gibbs free energy of adsorption,

$$\Delta G_a = \Delta H_a - T\Delta S_a \quad (6)$$

depends on the temperature and on the gas pressure. The dependence on pressure, p, arises from the translational partition function in the entropy of the gas-phase alkene,

$$S(T, p) = S(T, p_0) - R\ln(p/p_0). \quad (7)$$

Standard values are obtained with Eqs. (3)–(6) with $p_0 =$ 1 atm. The adsorption constant $K_a(T)$ is obtained from the standard Gibbs free energy, $\Delta G_a^0(T)$,

$$K_a = -RT\ln\Delta G_a^0, \quad (8)$$

and the surface coverage per Brønsted site, Θ, at a given partial pressure is obtained from Henry's law,

$$\Theta = K_a(T)p. \quad (9)$$

2.3. Force fields used in QM/MM

For the ion-pair shell-model description of the zeolite structures, all parameters are taken from [30]. For the interactions between the zeolite framework and the hydrocarbon, Lennard–Jones 6-12 parameters were taken from the consistent valence force field (CVFF) [45,46]. The choice of the atomic point charges for the hydrocarbon species deserves special attention. We derived fixed-point charges (point charge model, PCM) for each alkoxide and hydrocarbon molecules from the charges obtained by fitting their electrostatic potential (ESP). Geometries were first optimized with the use of TURBOMOLE. The Gaussian98 software [47] with the B3LYP functional and the triple-zeta/double-zeta plus polarization (TZP/DZP) basis sets [48] for oxygen atoms/all other atoms were used to obtain the ESP fit. For alkoxide surface species the free $H_3SiO(R)Al(OH)_2OSiH_3$ cluster model ($R = C_nH_{2n+1}$) was used. For this model, the charges obtained for the atoms of the hydrocarbon part $R = C_nH_{2n+1}$ add up to +0.4 (see Table 1), and the charges on the atoms of the zeolite part of the model add up to −0.4. However, this is not compatible with the assumptions of the ion-pair shell-model potential for the zeolite framework, which imply a total charge of −1 for the zeolite part of a surface alkoxide. We therefore increase the charges on the C_nH_{2n+1} hydrocarbon part until they add up to +1. We also constrain the charges of all atoms of the same type to be the same. For a given alkyl species, first the charges of all H atoms in C–H bonds are set to 0.1, and then the charges of the different types of C atoms are incremented. For the tertiary alkyl species, the charges of the C atoms in CH_3 groups are set to −0.2, and the charge of the C atom in the C–O alkoxide bond is set to 0.7 (Table 1). The final point-charge models for all studied hydrocarbon species are available in as supplementary material. The PCM has an effect on the stability of the adsorbed species, but test calculations showed that the difference between different point-charge models is rather small.

Table 1
Point charge models for *tert*-butoxide and isobutene compared to the charges obtained by the ESP fit

tert-Butoxide			Isobutene		
Atom	Charge by ESP fit	Point charge model used	Atom	Charge by ESP fit	Point charge model used
C (O–C)	0.64	0.7	C ($=CH_2$)	0.17	0.16
C (CH_3)	−0.27/−0.28/−0.30	−0.2	C (=C<)	−0.50	−0.5
H	0.05–0.08	0.1	C (CH_3)	−0.09	−0.07
H (average)	0.068		H($H_2C=$)	0.16	0.15
Total	0.4	1.0	H (others)	0.03	0.03

2.4. Details of the H-FER structure studied

The zeolite framework used in this study is H-FER (ferrierite). Experimental structural data are available only for a cation-exchanged and hydrated FER zeolite of the (approximate) composition $[Mg_2Na_2(H_2O)_{18}][Al_6Si_{30}O_{72}]$ [49]. The simulation cell ($a = 19.156$, $b = 14.127$, $c = 14.978$ Å) was constructed from these data. The unit cell was doubled in the z direction to ensure sufficient separation between the periodic images of the hydrocarbon species. All but one tetrahedral site were occupied with Si atoms. The resulting cell composition was $AlSi_{71}O_{144}$ (Si/Al ratio of 71). The aluminum was chosen to be in the T^2 position (the atom numbering in this study follows [49]). With Al at T^2 oxygen sites, O^7 and O^1 belong to the AlO_4 tetrahedron and, hence, are possible sites for alkoxide species. This is a reasonable choice because O^1 and O^7 (see Fig. 2) are located close to the intersection of the 8-membered ring (8-MR) and 10-MR pores. The cell of H-FER with the proton attached to oxygen O^1 was first optimized with the use of the shell-model ion-pair potential alone (GULP program) at constant pressure. The cell parameters (Å, degree) were $a = 18.70$, $b = 14.17$, $c = 14.96$, $\alpha = 89.84$, $\beta = 89.76$, and $\gamma = 90.00$. Haase and Sauer have optimized the same H-FER cell with the use of an earlier parameterization of the shell-model ion-pair potential based on Hartree–Fock data and obtained $a = 19.00$, $b = 14.31$, $c = 15.12$, $\alpha = 90.04$, $\beta = 89.75$, and $\gamma = 90.02$ [50]. The calculated cell parameters are not directly comparable with the experimental parameters because of the different cell compositions.

Table 2
Deprotonation energies (kJ/mol) for H-FER

Proton attached to	QM/MM hybrid		
	QM/MM	QM[a]	MM[b]
O^7	1218	1372	−154
O^1	1176	1344	−168

[a] DFT contribution to the QM/MM energy.
[b] Force field contribution to the QM/MM energy.

3. Results

3.1. Deprotonation energies and OH frequencies of free Brønsted sites

The deprotonation energy (a measure of acidity) of H-FER was calculated by the QM/MM embedded cluster approach for the proton located at the framework oxygen sites O^7 and O^1. The results are given in Table 2. If the proton is attached to oxygen O^7, the deprotonation energy is 42 kJ/mol higher, 1218 kJ/mol, indicating a more stable site. Calculations with periodic boundary conditions with the BP86 functional yield a deprotonation energy of 1236 kJ/mol for the O^7 site [51], whereas the present QM/MM method yields 1213 kJ/mol with this functional.

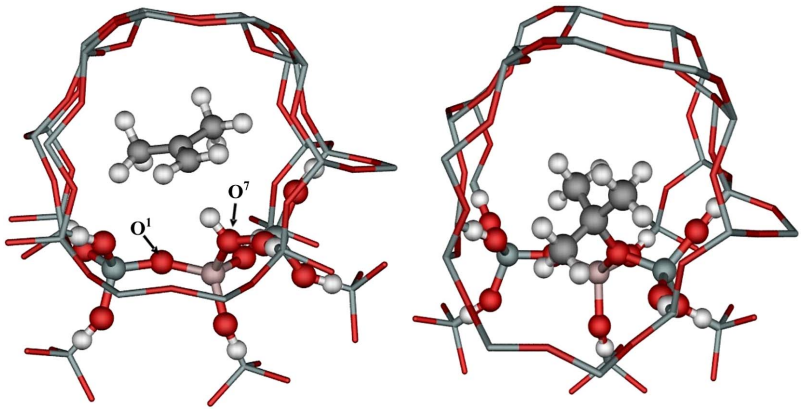

Fig. 2. Structures of adsorbed isobutene (π-complex, left) and chemisorbed *tert*-butyl alkoxide (right) optimized by QM/MM embedded cluster calculations. The QM cluster is drawn as ball-and-stick model. Proton and alkoxide are attached to oxygen O^7 (Al at T^2).

The small difference of 23 kJ/mol, which may be due partially to a different (plane wave) basis set and the use of an effective core potential (norm-conserving pseudopotential), supports the use of the hybrid QM/MM method.

The calculated O–H (O–D) stretching frequencies for unloaded H-FER are 3598 (2618) and 3418 (2485) cm^{-1} for the O^7H and O^1H surface hydroxyls, respectively. Comparison with the observed O–H (O–D) bands [16] at 3609 (2663) cm^{-1} shows that the O^7 proton position is indeed preferred to O^1 in H-FER.

3.2. Adsorption complexes

Table 3 shows the results for the adsorption complexes (π-complexes) of ethene, propene, 1-butene, isobutene, 1-pentene, and 2-methyl-1-butene at the O^1H and O^7H Brønsted sites. The adsorption energies are calculated as the difference between the total energy of the complex and the sum of the energies of the separated fragments [Eq. (2)]. We do not use the term "physisorption" for the π-complexes, even if they are van der Waals surface complexes [52], to avoid confusion with another (weaker) type of van der Waals complex not considered in this study, in which alkenes bind via their methyl groups with the Brønsted sites or in which alkenes bind to the silica part of the zeolite surface. Fig. 2 (left) shows the structure of isobutene adsorbed on the O^7H Brønsted site. The distances between the O^7H Brønsted proton and the midpoint of the C=C bond of the adsorbed alkenes vary between 221 and 243 pm. For the O^1H adsorption site the corresponding distances are longer. The longest distances, 277 and 350 pm, are found for the branched alkenes isobutene and 2-methyl-1-butene, respectively. Because of steric repulsions between the bulky branched hydrocarbons and the zeolite framework, the C=C double bond cannot get into an optimum position for interaction with the OH group. The energies of adsorption vary between 41 and 70 kJ/mol for adsorption at O^7H. For adsorption at O^1H a larger variation is observed, from 33 to 83 kJ/mol. For the linear alkenes, the adsorption energies increase with increasing carbon number, except for propene and 1-butene adsorbed on O^7H. The adsorption energies for 1-butene and 1-pentene at O^1H are particularly high, 81 and 83 kJ/mol, respectively, but these complexes are still 13 and 29 kJ/mol, respectively, less stable than the corresponding complexes at O^7H because the O^7H site is 42 kJ/mol more stable than the O^1H site. For comparison with observed values, we also calculate zero-point vibrational energy differences in adsorption and thermal contributions to the enthalpies. For linear and branched alkenes the heats of adsorption at 298 K are 5–7 kJ/mol and 8–10 kJ/mol smaller, respectively, than the energies of adsorption.

Table 3
Energies, ΔE_a; zero-point vibrational energies, ΔE_{ZPV}; enthalpies, ΔH_a^0; and entropy contributions to the Gibbs free energies,[a] $-T\Delta S_a$ (kJ/mol), at standard conditions (298 K, 1 atm) for adsorption of C_2 to C_5 alkenes at O^7H and O^1H sites in H-FER

	R(H–M)[b]	ΔE_a	MM[c]	QM[d]	ΔE_{ZPV}	ΔH_a^o	$-T\Delta S_a^o$
H-FER(O^7)							
Ethene	234	−41	−34	−7	5.3	−36	40
Propene	233	−57	−52	−5	4.9	−51	45
1-Butene	235	−52	−56	4	6.0	−45	50
Isobutene	221	−49	−56	7	9.5	−41	61
1-Pentene	236	−70	−83	13	6.8	−64	54
2-Methyl-1-butene	243	−57	−60	4	13.4	−47	63
H-FER(O^1)							
Propene	233	−58	−60	2	3.1	−53	45
1-Butene	253	−81	−84	2	2.5	−76	46
Isobutene	277	−33	−43	10	9.3	−23	53
1-Pentene	225	−83	−111	28	4.5	−78	57
2-Methyl-1-butene	350	−33	−51	17	10.4	−23	60

[a] See Eq. (6).
[b] Distance between the Brønsted proton and the midpoint of the C=C bond.
[c] Force field contribution to the QM/MM energy.
[d] DFT contribution to the QM/MM energy.

Table 4 shows calculated vibrational frequencies of 1-butene and isobutene as isolated molecules in the gas phase and adsorbed at the O^7H Brønsted site in H-FER. The largest effect of π-complex formation is seen on the OH (OD) frequencies. They shift toward lower wavenumbers by 205 (147) cm^{-1} and 392 (296) cm^{-1} because of hydrogen bond formation with the C=C bonds of 1-butene and isobutene, respectively. Concomitantly, the C=C stretching frequencies in the alkenes shift by 14 cm^{-1} to lower wavenumbers. The ranges of the C–H stretching frequencies shift only slightly to higher wavenumbers.

3.3. Chemisorption complexes (alkoxides)

Fig. 2 (right) shows the tertiary alkoxide structure obtained when isobutene chemisorbs at O^7. Table 5 shows the results for the alkoxide structures at the O^7 and O^1 sites of FER. The C–O(zeolite) bond distances and the energies of alkoxide formation, ΔE_{alk}, with respect to the alkene separated from the H(O^7)-FER zeolite are given. The butoxides show some characteristic features. Secondary butoxides are less stable than primary butoxides and have longer C–O bonds. Their stabilities are very different at O^1 and O^7 sites. As expected, the tertiary butoxide at O^7 is the least stable with the largest C–O distance. At O^1 no stable tertiary alkoxide structure is found. The relative stabilities are obviously determined largely by steric effects, that is, repulsion between methyl groups and the zeolite wall.

Table 6 shows the calculated vibrational frequencies of different butoxides. Compared with the adsorbed butenes (Table 4), there are no OH(OD) bands and no C=C bands. The range of the CH stretching bands is similar. Because of interactions with the zeolite framework the C–H stretching vibrations of the CH_3 groups extend now to much higher wavenumbers (3032 to 3067 cm^{-1}) into the range in which the alkene type H–C= vibrations are found for the π-adsorption complexes. Particularly high frequencies of 3111 and 3204 cm^{-1} are found for the *tert*-butyl alkoxide at O^7 and the isobutyl alkoxide at the O^1 position, re-

Table 4
Selected stretching frequencies (cm^{-1}, scaled by 0.9614) for 1-butene and isobutene in the gas-phase and adsorbed at HO^7 sites in ferrierite

Stretching mode	1-Butene				Isobutene		
	Gas phase		Adsorbed		Gas phase		Adsorbed
	Calculated[a]	Observed[b]	Calculated	Observed[c]	Calculated[a]	Observed[d]	Calculated
C=C	1640 (13.2)	1645	1626	1627	1648 (21.3)	1661	1634
H–CH_2–	2889 (26.1)	(2851)	2906	2879	2893 (18.7)	2893	2922
	2910 (31.5)	(2908)	2925	2900	2898 (41.6)	2911	2933
	2931 (8.9)	2925	2946	2926	2934 (0.0)	2941	2963
	2970 (35.8)	2970	2982	2941	2936 (46.0)	2945	2968
	2975 (34.9)	2970	2998	2973	2983 (27.8)	2970	3056
H–C=	2993 (32.0)	(2970)	2999	2973			
symm-H_2–C=	3007 (5.1)	(2998)	3013		3011 (9.1)	2991	3008
asymm-H_2–C=	3086 (17.9)	3086	3106	3080	3086 (18.9)	3086	3090
H–O	3598	3609[e]	3393	–			3200
D–O	2618	2663[e]	2471	∼2350			2322

[a] Intensities in parenthesis (km/mol).
[b] IR (Raman in parenthesis), Ref. [58].
[c] IR, Ref. [16].
[d] IR, Ref. [59].
[e] Unloaded H-FER, Ref. [16].

spectively. These modes belong to C–H bonds with short C–H···$O_{framework}$ contacts of 2.19 and 2.16 Å, respectively, which indicates a tight fit of the CH_3 groups to the zeolite wall in these alkoxide structures.

For all alkyl species studied, the C–O bond distances increase in the order primary < secondary < tertiary alkoxide from 150 to 163 pm. For the secondary and branched primary alkoxides, the C–O bond distances are longer for species attached to O^1 than for species attached to O^7. The stability of the alkoxides decreases in the order primary > secondary > tertiary, and, as a rule, lower stabilities correlate with longer C–O bond distances. The chemisorbed (alkoxide) species are more stable than the adsorbed molecules (π-complexes). The QM/MM energies of alkoxide formation vary between 62 and 205 kJ/mol. The calculations on a free T3 cluster model indicate much lower stability and smaller changes in the stabilities for different species; the chemisorption energies vary between 29 and 46 kJ/mol for all of the alkoxides.

A comparison of the relative stabilities for the alkoxides bonded to O^7 as a function of increasing carbon numbers is presented in Fig. 3. Relative stabilities differ from the energies of alkoxide formation by the energy differences between the *iso*- and *n*-alkenes. They are obtained by the addition of −14 and −9 kJ/mol to the ΔE_{alk} values of Table 5 for alkoxides formed by chemisorption of isobutene and 2-methyl-1-butene, respectively. The relative stabilities increase with the chain length, if similar types of alkoxides are compared. For example, the relative stabilities of secondary propyl, butyl, and pentyl alkoxides are −137, −156, and −198 kJ/mol. The bulkiness of the adsorbed species explains the lower stability of specific alkoxides. For instance, among the primary ones, the isobutyl and 2-methylbutyl alkoxides are about 30 kJ/mol less stable than the corresponding linear alkoxides, regardless of the oxygen (O^1 or

Table 5
C–O bond distances (in pm) and energies of alkoxide formation at O^7 and O^1 sites in FER from alkenes and H-FER(O^7), ΔE_{alk} (kJ/mol). Given are also the DFT contribution, QM, and the force field contribution to the energy of alkoxide formation from the hypothetically separated FER^- anion and gas phase alkyl cation (step II, see text), MM(II)[a]

	R(C–O)	ΔE_{alk}[b]	QM[c]	MM-II[d]
Propyl (O^7)	151	−157	−17	14
Propyl (O^1)	151	−171	17	−34
Isopropyl (O^7)	154	−137	−4	22
Isopropyl (O^1)	157	−96	17	42
Butyl (O^7)	152	−190	+3	−39
Butyl (O^1)	152	−188	+7	−40
sec-Butyl (O^7)	155	−156	−5	3
sec-Butyl (O^1)	157	−108	32	15
Isobutyl (O^7)	151	−145	21	−11
Isobutyl (O^1)	154	−149	93	−88
tert-Butyl (O^7)	162	−62	73	20
Pentyl (O^7)	152	−194	17	−57
Pentyl (O^1)	152	−205	7	−58
1-Methylbutyl (O^7)	154	−198	2	−46
1-Methylbutyl (O^1)	157	−162	21	−29
1-Ethylpropyl (O^7)	155	−172	13	−31
1-Ethylpropyl (O^1)	156	−116	31	6
2-Methylbutyl (O^7)	150	−159	20	−24
2-Methylbutyl (O^1)	155	−157	38	−41
3-Methylbutyl (O^7)	150	−191	21	−57
3-Methylbutyl (O^1)	153	−157	38	−41
1,2-Dimethylpropyl (O^7)	155	−173	31	−49
l,2-Dimethylpropyl (O^1)	157	−121	36	−2
1,1-Dimethylpropyl (O^7)	163	−78	78	−2

[a] ΔE_{alk} = QM − 154 kJ/mol + MM(II).
[b] $\Delta E_{alk} = E$(alkoxide) − E(H-FER(O^7)) − E(alkene).
[c] DFT contribution to the QM/MM energy.
[d] Force field contribution to step II, ΔE(II) = E(alkoxide) − E(FER^-) − E(alkyl cation).

Table 6
C–H stretching frequencies (cm^{-1}, scaled by 0.9614) for butyl alkoxide species at O^1 and O^7 positions in FER

At O^7		At O^1		At O^7		At O^1
Butyl	*sec*-Butyl	Butyl	*sec*-Butyl	Isobutyl	*tert*-Butyl	Isobutyl
2893	2915	2901	2923	2903	2911	2914
2902	2919	2906	2931	2924	2915	2920
2927	2954	2930	2964	2956	2936	2957
2960	2962	2965	2982	2960	2966	2976
2974	2968	2966	2989	2981	2983	2981
2984	2980	2970	3003	2994	3029	2982
2993	2999	2982	3037	3004	3061	2999
2999	3017	3013	3050	3028	3080	3034
3047	3051	3032	3067	3058	3111	3204

O^7) to which they are bonded. As a result, the stabilities of the branched primary and secondary species are about the same as seen in Fig. 3 for C_4 and C_5 species. The tertiary species are relatively unstable compared with primary and secondary ones. The *tert*-butyl and 1,1-dimethylpropyl alkoxides (O^7) are 114 and 107 kJ/mol less stable, respectively, than the butyl and pentyl alkoxides (O^7). Furthermore, a hindered local geometry around the active site of the zeolite has a destabilizing effect on the bulkier alkoxides. Whereas the primary straight-chain alkoxide species are almost equal in stability at O^7 and O^1 sites, the stability of the bulkier species is lower at the hindered location O^1. For instance, the secondary straight-chain alkoxides are 38–50 kJ/mol less stable when bonded to O^1. The most pronounced effect of the hindered position on the bulky species can again be seen for tertiary alkoxides; no minima were found on the potential energy surface for *tert*-butyl and 1,1-dimethylpropyl alkoxides bonded to O^1.

The decreasing stability in the order of primary, secondary, and tertiary alkoxides is contrary to what is expected from the relative stability of primary, secondary, and tertiary carbenium ions. However, this becomes understandable if we decompose the alkoxide formation reaction,

$$\text{H-FER} + C_nH_{2n} \rightarrow C_nH_{2n+1}\text{–FER},$$

into two hypothetical steps: proton transfer from the Brønsted site to the alkene forming a carbenium ion separated from the deprotonated zeolite,

$$\text{H-FER} + C_nH_{2n} \rightarrow \text{FER}^- + C_nH_{2n+1}{}^+, \quad (11)$$

and formation of the alkoxide by C–O bond formation between the carbenium ion and the negatively charged zeolite surface site,

$$\text{FER}^- + C_nH_{2n+1}{}^+ \rightarrow H_{2n+1}C_n\text{–FER}. \quad (12)$$

The energy of the first reaction is given by the difference between the deprotonation energy of the zeolite (DP) and the proton affinity (PA) of the alkene,

$$\Delta E(\text{I}) = \text{DP(H-FER)} - \text{PA(alkene)}.$$

The energy of the second step, $\Delta E(\text{II})$, includes the energy of C–O bond formation and any van der Waals interaction between the alkoxide residues and the zeolite wall. The energy of alkoxide formation is

$$\Delta E_{\text{alk}} = \Delta E(\text{I}) + \Delta E(\text{II}).$$

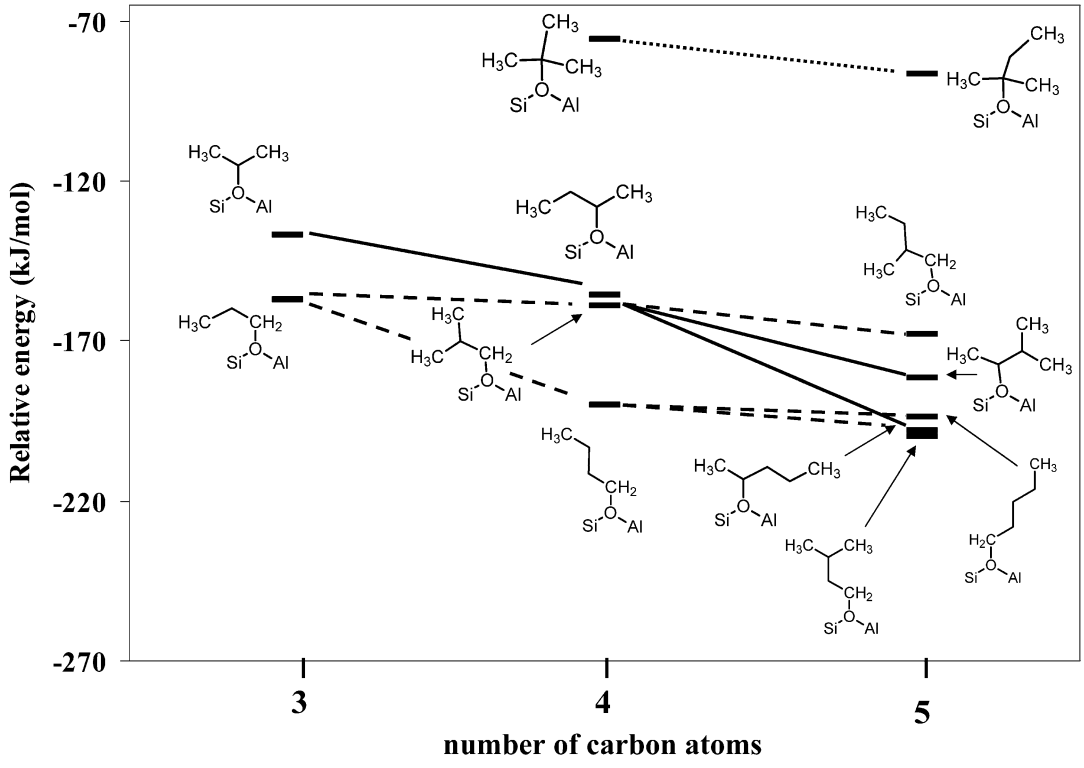

Fig. 3. Relative stabilities of alkoxide species at O^7 as a function of the carbon number.

Table 7
Decomposition of energy of alkoxide formation into (I) formation of a hypothetical ion pair FER^- and alkyl cation, and (II) formation of the alkoxide from the ion-pair. Given are also the QM and MM contributions to these energies (kJ/mol)

FER^- + cation	PA(alkene)[a]	ΔE(I)[b]	QM(I)[c]	ΔE(II)[d]	QM(II)[e]	MM(II)[f]
Isopropyl	783	435	589	−572	−593	+22
sec-Butyl	799	419	573	−575	−578	+3
1-Methylbutyl	811	406	561	−605	−559	−46
tert-Butyl	843	374	529	−436	−456	+20
1,1-Dimethyl-propyl	855	362	516	−440	−438	−2

[a] Proton affinity.
[b] Energy of reaction I.
[c] DFT contribution to the energy of reaction (I), the force field contribution is −154 kJ/mol for all cases.
[d] Energy of reaction II.
[e] DFT contribution to the energy of reaction II.
[f] Force field contribution to the energy of reaction II.

Table 7 shows ΔE(I) and ΔE(II) for the formation of selected secondary and tertiary alkoxides on O^7 from the corresponding alkenes (see Table 5 for the ΔE_{alk} values). First we note that primary carbenium ions do not exist as (meta-)stable species in the gas phase. Protonation of *n*-alkenes yields secondary carbenium ions (isopropyl, *sec*-butyl, and 1-methylbutyl cations), and protonation of isobutene and 2-methyl-1-butene yields tertiary carbenium ions (*tert*-butyl and 1,1-dimethylpropyl cations). Table 7 shows that the PA of the *n*-alkenes increases with the carbon number. The PA's of isobutene and 2-methyl-1-butene are 44 kJ/mol larger than those of the corresponding *n*-alkenes. Since the DP of the zeolite is the same for a given framework position, the changes in ΔE(I) reflect the changes in the PA of the alkene.

Formation of the alkoxides from the separated ions in the gas phase is an exothermic process, and ΔE(II) is largely determined by the QM contribution because the charged species (positively charged carbenium ion and negatively charged deprotonated site) are part of the embedded QM cluster, and formation of the C–O bond also occurs within the QM cluster. The MM contribution to ΔE(II), MM(II), is much smaller. It describes the attractive or repulsive interactions between the methyl (or methylene) groups and the zeolite wall.

For the formation of secondary alkoxides the changes of ΔE(I) and of ΔE(II) both contribute to the increasing stability with increasing carbon number (−137, −156, and −198 kJ/mol for C_3, C_4, and C_5). The tertiary butyl and pentyl alkoxides are 80 and 111 kJ/mol less stable than the corresponding secondary alkoxides. The force-field part of ΔE(II), MM(II), which includes the repulsion between the methyl groups and the zeolite wall, contributes +17 and +44 kJ/mol, respectively, whereas the QM(II) part is repulsive (+122 and +121 kJ/mol, respectively) because the repulsion does not permit the C–O(zeolite) bond to be short enough for optimum binding (162 and 163 pm compared with 155 and 154 pm; see Table 5). These effects overcompensate for the larger stability of the tertiary cations compared with the secondary *n*-alkyl cations, which contributes −44 kJ/mol (see the PA and ΔE(I) values).

We also use the decomposition into reactions I and II to estimate the uncertainty of our alkoxide formation energy due to the choice of the van der Waals parameters. Note that the lion's share of ΔE(II) comes from the DFT calculation on the embedded cluster, QM(II). The force field (van der Waals interactions between the hydrocarbon and the zeolite wall) makes only a small contribution, MM(II). We have included MM(II) in Table 5 for all alkoxide structures studied. The largest MM(II) value in Table 5 is −88 kJ/mol. Assuming an error of 10% for MM(II), the estimated uncertainty of ΔE(II) due to the van der Waals parameters is ±10 kJ/mol. The MM contribution of ΔE(I), MM(I), comes from the deprotonation energy of the zeolite (Table 2) and is constant for all alkoxide species at a given framework position (−154 kJ/mol for O^7). We have repeatedly shown that our hybrid QM/MM approach yields very reliable results for deprotonation energies of zeolites that are stable with respect to increasing cluster size [20,30]. Hence, MM(I) = −154 kJ/mol is accurately known for a given QM level, and its estimated uncertainty is ±5 kJ/mol. Since

$$\Delta E_{alk} = \Delta E(\mathrm{I}) + \Delta E(\mathrm{II}) = \mathrm{QM} - 154\ \mathrm{kJ/mol} + \mathrm{MM(II)},$$

the estimated uncertainty of ΔE_{alk} due to force-field parameters is ±15 kJ/mol. Small changes in the van der Waals parameters will not change the predicted large stability of the alkoxide species.

3.4. Free cluster model calculations

Without embedding, the T3 cluster calculations cannot distinguish between OH groups at different crystallographic sites, for example, between the O^7 and O^1 sites. They yield a deprotonation energy (1303 kJ/mol) that is about 100 kJ/mol larger than the QM/MM result. The energies of adsorption (π-complex) are between 19 and 21 kJ/mol for C_3 to C_5 hydrocarbons, significantly less than the QM/MM results of Table 3, which also show a much larger variation between 33 and 83 kJ/mol. Calculations using the free T3 cluster predict alkoxides to be more stable than the adsorption complexes (alkoxide formation energies between −20 and −46 kJ/mol), but absolute values are again much too low. Important trends in alkoxide formation energies are not reproduced; the same value (−40 kJ/mol) is obtained for the propyl, butyl, and pentyl species. For the secondary alkoxides marginally larger values are obtained, −46, −44, and −43 kJ/mol for isopropyl, *sec*-butyl, and 1-methylbutyl species, respectively, whereas −30 kJ/mol are obtained for the 1-ethylpropyl alkoxide. Among the primary species, isobutyl (−23 kJ/mol), 2-methylbutyl (−21 kJ/mol), and 3-methylbutyl (−28 kJ/mol) are less stable than the corresponding unbranched alkoxides, but the large stability loss of tertiary species is not seen in the free T3 cluster results (−24 and −20 kJ/mol for *tert*-butyl and 1,1-dimethylpropyl alkoxides).

4. Discussion

Before we start the discussion we remind the reader that our calculations refer to a high Si/Al ratio of 71 with distances of about 15 Å between Brønsted sites (i.e., to a very low site density).

4.1. Heats of adsorption

There is a lack of experimental results for heats of adsorptions of alkenes on protonic zeolites. The reason for this is probably the oligomerization of olefins over acidic zeolites. This process could be suppressed at low temperatures, but then adsorption is extremely slow, and it is very difficult to reach adsorption equilibrium. Heats of adsorption have been measured only for alkanes; for example, Lercher et al. report heats of adsorption of propane, *n*-butane, and *n*-pentane in H-FAU (33, 40, and 47 kJ/mol, respectively) [53,54] and H-FER (49, 59, and 69 kJ/mol, respectively) [55]. The values for H-FER are larger than for H-FAU because in H-FER there is a better fit of the hydrocarbon onto the zeolite wall. If we assume a constant increment for additional CH_2 groups of +7 and +10 kJ/mol for H-FAU and H-FER, respectively, we get estimates for ethane in H-FAU and H-FER of 26 and 39 kJ/mol. We expect that the results for the corresponding alkenes will be not very different. The presence of a CH=CH double bond instead of a CH_2–CH_2 single bond will reduce the nonspecific (dispersion) interaction because there are two C–H bonds less, but there will be an additional specific (electrostatic) interaction between the OH group and the double bond in acidic zeolites. This is supported by the only available experimental value for an alkene, ethene adsorbed on H-Y zeolite (that still contains Na^+ ions), 35.1 ± 1.3 kJ/mol [56], which is indeed in the above-mentioned range.

Hence, we expect heats of adsorption between 26 and 39 kJ/mol for ethene, between 33 and 49 kJ/mol for propene, between 40 and 59 kJ/mol for butenes, and between 47 and 69 kJ/mol for pentenes, depending on the fit of the hydrocarbon to the zeolite wall. In these estimates we use the H-FAU results as a lower limit representing a poor fit to the zeolite wall. The results of the QM/MM embedded cluster calculations for the heats of adsorption (298 K) at the O^7H site of ethene (36 kJ/mol), propene, 1-butene (45 kJ/mol), and 1-pentene (64 kJ/mol) fall into the expected ranges. The value for propene (51 kJ/mol) is slightly above the expected range. From the results of Lercher et al. for H-MFI [53,54] we also know that the heats of adsorption for isobutane and isopentane are 6 kJ/mol lower than the values for the corresponding *n*-alkanes. The calculated heats of adsorption of isobutene and 2-methyl-1-butene at O^7H (41 and 47 kJ/mol, Table 3) are also lower by 4 and 7 kJ/mol, respectively, than those of the corresponding *n*-alkenes. The values for isobutene and 2-methyl-1-butene at site O^1 are very low (23 kJ/mol for both), which is understandable because of the long distance between the proton and the midpoint of the C=C bond caused by the steric repulsion.

Plane-wave DFT calculations with periodic boundary conditions typically give values for adsorption energies that are too low [57], because the density functionals used do not properly account for the weak van der Waals interactions (dispersion forces). In a fully periodic DFT study (PW91 functional), energies of 33, 38, and 45 kJ/mol have been obtained for the adsorption, respectively, of propene, 1-butene, and 1-pentene in H-gmelinite [57]. The corresponding heats of adsorption, 27, 32, and 39 kJ/mol, respectively (we are using thermodynamic corrections of 6 kJ/mol; cf. Table 3) are lower than the lower limits of the experimental estimates above. Our hybrid QM/MM method describes the majority of the interactions between the hydrocarbon and the zeolite wall by the force field, which is superior to DFT in describing van der Waals interactions. Table 3 shows the contributions of the QM part and the MM part to the adsorption energy. Dispersion (described by the force field) is the dominating stabilizing contribution that determines the adsorption structures, whereas the specific OH-double bond interaction (described by DFT) plays a minor role. Hence, in the adsorption structure the dispersion (force field) contribution is maximized, which explains the observation that for the longer alkenes the QM contribution is not even attractive.

4.2. Vibrational frequencies of adsorbed butenes

For gas-phase 1-butene and isobutene the calculated frequencies generally show good agreement with available experimental data (Table 4) [58,59]. The observed C=C stretching frequencies, 1645 cm^{-1} for 1-butene and 1661 cm^{-1} for isobutene, correspond to calculated values of 1640 and 1648 cm^{-1}, respectively. The observed H–C stretching frequencies are in the range of 2851–3086 cm^{-1} for 1-butene and 2879–3080 cm^{-1} for isobutene, whereas calculated values are in the ranges of 2889–3086 cm^{-1} and 2906–3106 cm^{-1}, respectively.

Comparison of the calculated O–H (O–D) stretching frequencies for the unloaded zeolite, 3418 (2485) and 3598 (2618) cm^{-1} for the proton at the O^1 and O^7 positions, respectively, with the observed bands at 3609 (2663) cm^{-1} [16] shows that O^7 is the preferred proton position. On adsorption of 1-butene and isobutene, the OD band broadens and shifts to lower wavenumbers by about 300 cm^{-1} [16] and 416 cm^{-1} (measured for adsorption of isobutene in D-MOR) [14], respectively. The calculations reproduce the shift qualitatively, yielding 150 cm^{-1} for 1-butene and 300 cm^{-1} for isobutene (Table 4). The calculated ν(C=C) shift of −14 cm^{-1} is supported by observed shifts of −18 cm^{-1} (1-butene, Table 7) [16] and −23 cm^{-1} (1638 cm^{-1} observed for isobutene in H-MOR) [14].

4.3. Stability of the alkoxide species

The major finding of this study is the relatively high stability of the primary and secondary alkoxide species compared with adsorbed alkenes. Even the tertiary butoxides and pentoxides are more stable by 14 and 21 kJ/mol, respectively, than the isobutene and 2-methyl-1-butene adsorption complexes. A previous hybrid QM/MM study of isobutene adsorption on H-FAU has also found that *tert*-butyl alkoxide is 40 ± 5 kJ/mol more stable than the adsorption complex [60]. The *tert*-butoxide is more stable in H-FAU (95 ± 5 kJ/mol) [60] than in H-FER at O^7 (62 kJ/mol, Table 5), which suggests that the steric repulsions for tertiary alkoxide species are more pronounced in H-FER compared with H-FAU.

The isopropyl, *sec*-butyl, and 2-methylbutyl alkoxides are 80, 104, 128 kJ/mol more stable, respectively, than the corresponding π-complexes; and the isobutyl and 2-methylbutyl alkoxides are 95 and 102 kJ/mol more stable than the isobutene and 2-methyl-1-butene π-complexes, respectively. The energy gain on alkoxide formation from the π-complexes is less for the more bulky isobutene and 2-methyl-1-butene molecules because in the alkoxide they have to get so close to the zeolite surface to form the C–O bond that the repulsive range of the interactions between methyl (or methylene) groups in the alkoxide and the zeolite wall is reached. Hence, the present QM/MM results do not support the assumption [5] that the van der Waals stabilization is constant for all hydrocarbon structures once the hydrocarbon is inside the zeolite.

Much smaller energy preferences for chemisorbed species are predicted by pure density functionals for periodic structures or by free cluster calculations. PW91 calculations for gmelinite (periodic boundary conditions) [57] predict that isopropyl, *sec*-butyl, and 1-methylbutyl species are more stable by 33, 25, and 13 kJ/mol than the π-complexes. PBE calculations for isobutene in H-FER [61] indicate that isobutyl alkoxides are 14 kJ/mol less stable than adsorbed isobutene. B3LYP calculations for MFI (cluster calculations) [62] predict that isopropyl and 1-methylpentyl alkoxides are only 16 and 9 kJ/mol more stable than adsorbed propene and 1-hexene, respectively. This is similar to the present results for the free T3 cluster model.

Our results also contradict the conclusion of [62] "that the stability of the alkoxide species does not depend significantly on the carbon number." The dependence on the carbon number is clearly seen in Fig. 3. In addition, the stability of alkoxides depends on possible steric effects connected with the branching of the hydrocarbon skeleton and on the adsorption site. The formation of tertiary alkoxide species is particularly difficult (see also [63]), and sometimes their formation is just impossible, as found in this study for the O^1 position in FER. Neither the size dependence of the relative stability nor the variation with different sites can be predicted from nonembedded small cluster models. Examples of the drastic effects of the local environment of the active site on the stability of chemisorbed species have been reported previously [11,13,63].

Table 8
Energies, ΔE_{alk}, zero-point vibrational energies, ΔE_{ZPV}, standard enthalpies, ΔH^o_{alk}, and standard entropy contributions to the Gibbs free energies,[a] $-T\Delta S^o_{alk}$ (kJ/mol) at 623 K and 1 atm for alkoxide formation from 1-butene and isobutene at O^7 and O^1 sites in ferrierite

	ΔE_{alk}[a]	ΔE_{ZPV}	ΔH^o_{alk}	$-T\Delta S^o_{alk}$
			623 K	623 K
Butyl (O^7)	−190	18	−176	131
Butyl (O^1)	−188	13	−175	123
sec-Butyl (O^7)	−156	15	−143	136
sec-Butyl (O^1)	−108	13	−95	133
Isobutyl (O^7)	−145	19	−130	137
Isobutyl (O^1)	−149	16	−134	135
tert-Butyl (O^7)	−62	14	−59	131

[a] Alkoxide formation from H-FER(O^7) and gas phase butene, $E_{alk} = E - E(\text{H-FER}(O^7)) - E(\text{butene})$.

Finally, we would like to present an argument that alkoxide stabilities as large as 150–200 kJ/mol are reasonable values for primary and secondary butyl and pentyl species if these species play a role in alkene transformation reactions. The reaction temperature for the skeletal isomerization of linear butenes is about 623 K, and for this temperature we have calculated the standard (1 atm) heat of adsorption and the standard entropy of adsorption for the C_4 species. These values are included in Table 5. The entropy loss on chemisorption of butenes at O^7H makes a contribution ($-T\Delta S^o_{alk}$) to the Gibbs free energy of adsorption of around 134 ± 3 kJ/mol (Table 8). To achieve an occupation of the available O^7H Brønsted sites of $\Theta = 1/100$ or more at an alkene pressure of 1 atm ($\Delta G^o_{alk} = +24$ kJ/mol, Eqs. (8) and (9)), we need $-\Delta H^o$ values of 110 ± 3 kJ/mol or larger. This means that the stabilization energy should exceed 123 ± 3 kJ/mol. To achieve the same site occupation at a lower partial pressure, the stabilization energy needs to be about 12 kJ/mol larger for each order-of-magnitude pressure decrease. The stabilization energies of the butyl, the isobutyl, and the *sec*-butyl alkoxides are all above these limits, and these species would have a significant concentration in H-FER even at 623 K. In contrast, the stabilization energy of the *tert*-butyl species (−62 kJ/mol) would yield only a negligible surface coverage on the order of $\Theta = 10^{-7}$ for 1 atm and 623 K.

4.4. Impact of the stable alkoxide species on the chemical reactions

The fact that primary and secondary alkoxide species are much more stable than the corresponding adsorbed alkenes has consequences for the energy profile of the monomolecular skeletal isomerization of linear alkenes. Typically, DFT calculations for large clusters or on periodic structures (periodic boundary conditions) predict chemisorbed species only marginally more stable or even less stable than the adsorbed

species [4,11,13,62]. According to the reaction scheme proposed by Boronat et al. [3,4] (see Fig. 1), the following species would be involved in the isomerization of 1-butene on H-FER: adsorbed 1-butene (O^1H), *sec*-butoxide (O^7), isobutoxide (O^1), and, finally, adsorbed isobutene (O^7H). The corresponding energies relative to H(O^7)-FER + 1-butene obtained by our QM/MM study are (Tables 3 and 5) −52, −108, −159, and −55 kJ/mol, respectively. The *sec*-butoxide has been reported to be ∼ 30 kJ/mol less stable than the adsorbed 1-butene (cluster C) [4], whereas here it is favored by about 50 kJ/mol. Consequently, the apparent energy barrier, the energy difference between the transition structure and adsorbed 1-butene, may significantly decrease compared with that reported previously [4] if the intrinsic barrier is about constant. The apparent activation energy could decrease even to the level of the adsorption/desorption step of the molecules. This is in accordance with the literature. In their kinetic study of butene isomerization over H-FER zeolite [64], Domokos et al. found an apparent activation energy of about 60 kJ/mol, which is very close to the isobutene desorption enthalpy. For the isomerization of linear pentene, which supposedly is the rate-determining step in the isomerization of *n*-pentane, DFT(PW91) calculations with periodic boundary conditions suggest an intrinsic energy barrier of 98–110 kJ/mol [5]. Experimentally a value as low as 55 kJ/mol has been reported [65]. This discrepancy may be explained by the high stability of pentoxide species, which are relevant intermediates in the isomerization. According to the present hybrid DFT/force-field calculations the 1-methylbutoxide is 128 kJ/mol more stable than the adsorbed 1-pentene, but only 13 kJ/mol according to the PW91 calculations [5].

The presence of the very stable alkoxide may also affect the energy profiles of other proposed reactions. Recently it has been concluded that knowledge of the stability of alkoxide species relative to adsorbed alkenes will be necessary for discrimination between two mechanistic proposals for the dimerization of linear alkenes, that is, concerted or stepwise reactions [66]. In the stepwise mechanism first an alkoxide is formed, whereas the concerted mechanism assumes that protonation and C–C bond formation occur simultaneously in a single step without formation of an alkoxide. As described above, the apparent activation energy in the stepwise mechanism is supposed to decrease because of stable alkoxide intermediates, if the reaction barrier is assumed to be of the same order of magnitude.

5. Conclusions

Contrary to full DFT calculations, hybrid DFT/force-field calculations on embedded cluster models make reliable predictions for the heats of adsorption of alkenes. The values obtained fall into ranges inferred for alkenes from experimental values for alkanes in H-FER and H-FAU. The present study predicts that primary and secondary alkoxide species are significantly more stable than adsorbed alkenes and that the chemisorption energy increases with increasing carbon number if alkoxides of the same type are compared. For example, the enthalpy of chemisorption of 1-butene at 623 K is about 175 kJ/mol. The stabilities of the adsorbed alkenes and the alkoxide species depend on the local environment around the active site. Tertiary alkoxide species are much less stable than primary or secondary ones or even nonexistent when bonded to sterically constricted sites. The presence of stable alkoxide species has an effect on the apparent activation energies of hydrocarbon transformation reactions over H-zeolites, if alkoxides play a role as intermediates. In the monomolecular reaction mechanism of the skeletal isomerization of linear butenes and pentenes, the presence of very stable primary and secondary alkoxide intermediates in the reaction path could reduce the apparent activation barrier to the level of the adsorption/desorption steps.

Acknowledgments

This work has been supported by the Deutsche Forschungsgemeinschaft within the Priority Program 1155. Financial support for V.N. from the Graduate School of Materials Research, Fortum Foundation, and Stiftelsens för Åbo Akademi forskningsinstitut is greatly acknowledged.

Supplementary Material

The online version of this article contains additional supplementary material.

Please visit DOI:10.1016/j.jcat.2005.01.035.

References

[1] V.B. Kazansky, Catal. Today 51 (1999) 419.
[2] J.F. Haw, J.B. Nicholas, T. Xu, L.W. Beck, D.B. Ferguson, Acc. Chem. Res. 29 (1996) 259.
[3] M. Boronat, P. Viruela, A. Corma, J. Phys. Chem. A 102 (1998) 982.
[4] M. Boronat, P. Viruela, A. Corma, Phys. Chem. Chem. Phys. 3 (2001) 3235.
[5] T. Demuth, X. Rozanska, L. Benco, J. Hafner, R.A. van Santen, H. Toulhoat, J. Catal. 214 (2003) 68.
[6] P. Meriaudeau, C. Naccache, Adv. Catal. 44 (1999) 505.
[7] J. Houzvicka, V. Ponec, Catal. Rev. Sci. Eng. 39 (1997) 319.
[8] S. van Donk, J.H. Bitter, K.P. de Jong, Appl. Catal. A 212 (2001) 97.
[9] D. Rutenbeck, H. Papp, H. Ernst, W. Schwieger, Appl. Catal. A 208 (2001) 153.
[10] A.G. Stepanov, M.V. Luzgin, S.S. Arzumanov, H. Ernst, D. Freude, J. Catal. 211 (2002) 165.
[11] X. Rozanska, R.A. van Santen, T. Demuth, F. Hutschka, J. Hafner, J. Phys. Chem. B 107 (2003) 1309.
[12] P.E. Sinclair, A. de Vries, P. Sherwood, C.R.A. Catlow, R.A. van Santen, J. Chem. Soc., Faraday Trans. 94 (1998) 3401.
[13] M. Boronat, C.M. Zicovich-Wilson, P. Viruela, A. Corma, J. Phys. Chem. B 105 (2001) 11169.
[14] H. Ishikawa, E. Yoda, J.N. Kondo, F. Wakabayashi, K. Domen, J. Phys. Chem. B 103 (1999) 5681.
[15] J.B. Nicholas, J.F. Haw, J. Am. Chem. Soc. 120 (1998) 11804.

[16] E. Yoda, J.N. Kondo, F. Wakabayashi, K. Domen, Appl. Catal. A 194–195 (2000) 275.
[17] F.C. Meunier, L. Domokos, K. Seshan, J.A. Lercher, J. Catal. 211 (2002) 366.
[18] C. Pazè, B. Sazak, A. Zecchina, J. Dwyer, J. Phys. Chem. B 103 (1999) 9978.
[19] M. Sierka, J. Sauer, J. Chem. Phys. 112 (2000) 6983.
[20] L.A. Clark, M. Sierka, J. Sauer, J. Am. Chem. Soc. 125 (2003) 2136.
[21] L.A. Clark, M. Sierka, J. Sauer, J. Am. Chem. Soc. 126 (2004) 936.
[22] M. Sierka, J. Sauer, J. Phys. Chem. B 105 (2001) 1603.
[23] M. Davidová, D. Nachtigallová, P. Nachtigall, J. Phys. Chem. B 108 (2004) 13674.
[24] S.T. Bromley, C.R.A. Catlow, T. Maschmeyer, CATTECH 7 (2003) 164.
[25] F. Jousse, L. Leherte, D.P. Vercauteren, Mol. Simul. 17 (1996) 175.
[26] F. Jousse, L. Leherte, D.P. Vercauteren, J. Mol. Catal. 119 (1997) 165.
[27] J.R. Maple, in: P. von Ragué Schleyer, N.L. Allinger, P.A. Kollman, T. Clark, H.F. Schaefer III, J. Gasteiger, P.R. Schreiner (Eds.), in: Encyclopedia of Computational Chemistry, vol. 2, Wiley, Chichester, 1998, p. 1025.
[28] J.-R. Hill, J. Sauer, J. Phys. Chem. 98 (1994) 1238.
[29] J.-R. Hill, J. Sauer, J. Phys. Chem. 99 (1995) 9536.
[30] M. Sierka, J. Sauer, Faraday Discuss. 106 (1997) 41.
[31] T.A. Wesolowski, O. Parisel, Y. Ellinger, J. Weber, J. Phys. Chem. A 101 (1997) 7818.
[32] S. Grimme, J. Comput. Chem. 25 (2004) 1463.
[33] A.H. Fuchs, A.K. Cheetham, J. Phys. Chem. B 105 (2001) 7375.
[34] A.D. Becke, Phys. Rev. A 38 (1988) 3098.
[35] C. Lee, W. Yang, R.G. Parr, Phys. Rev. B 37 (1988) 785.
[36] A.D. Becke, J. Chem. Phys. 98 (1993) 5648.
[37] A. Schäfer, C. Huber, R. Ahlrichs, J. Chem. Phys. 100 (1994) 5829.
[38] R. Ahlrichs, M. Bär, M. Häser, H. Horn, C. Kölmel, Chem. Phys. Lett. 162 (1989) 165.
[39] M. Häser, R. Ahlrichs, J. Comput. Chem. 19 (1989) 1746.
[40] M. von Arnim, R. Ahlrichs, J. Comput. Chem. 19 (1998) 1746.
[41] O. Treutler, R. Ahlrichs, J. Chem. Phys. 102 (1995) 346.
[42] J.D. Gale, J. Chem. Soc., Faraday Trans. 93 (1997) 629, Program GULP (General Utility Lattice Program), Royal Institution/Imperial College, London, 1992–1994.
[43] A.P. Scott, L. Radom, J. Phys. Chem. 100 (1996) 16502.
[44] C.J. Cramer, Essentials of Computational Chemistry – Theory and Models, Wiley, Chicester, 2002.
[45] A.T. Hagler, S. Lifson, P. Dauber, J. Am. Chem. Soc. 101 (1979) 5122.
[46] Original CVFF force field provided with the Discover program by Accelrys Inc. We use the 6-12 Lennard–Jones potential $V_{ij} = A_{ij}/r_{ij}^6 - B_{ij}/r_{ij}^6$ with a cut-off radius of 40 Å. The parameters for pair interactions A_{ij} and B_{ij} are combined from atomic parameters A_i, B_j as geometric means. The parameters are (A/eVÅ^6 and B/eVÅ^{12}): $A_{\mathrm{C}} = 77636.682813$, $B_{\mathrm{C}} = 22.917192$; $A_{\mathrm{H}} = 308.252900$, $B_{\mathrm{H}} = 1.425414$; $A_{\mathrm{O}} = 11833.862431$, $B_{\mathrm{O}} = 21.633477$; $A_{\mathrm{Si,Al}} = 136561.436222$, $B_{\mathrm{Si,Al}} = 30.788578$.
[47] M.J. Frisch, G.W. Trucks, H.B. Schlegel, G.E. Scuseria, M.A. Robb, J.R. Cheeseman, V.G. Zakrzewski, J. J. A. Montgomery, R.E. Stratmann, J.C. Burant, S. Dapprich, J.M. Millam, A.D. Daniels, K.N. Kudin, M.C. Strain, O. Farkas, J. Tomasi, V. Barone, M. Cossi, R. Cammi, B. Mennucci, C. Pomelli, C. Adamo, S. Clifford, J. Ochterski, G.A. Petersson, P.Y. Ayala, Q. Cui, K. Morokuma, N. Rega, P. Salvador, J.J. Dannenberg, D.K. Malick, A.D. Rabuck, K. Raghavachari, J.B. Foresman, J. Cioslowski, J.V. Ortiz, A.G. Baboul, B.B. Stefanov, G. Liu, A. Liashenko, P. Piskorz, I. Komaromi, R. Gomperts, R.L. Martin, D.J. Fox, T. Keith, M.A. Al-Laham, C.Y. Peng, A. Nanayakkara, M. Challacombe, P.M.W. Gill, B. Johnson, W. Chen, M.W. Wong, J.L. Andres, C. Gonzalez, M. Head-Gordon, E.S. Replogle, J.A. Pople, Gaussian 98, Revision A.11.3, Gaussian, Inc., Pittsburgh, PA, 2002.
[48] A. Schäfer, H. Horn, R. Ahlrichs, J. Chem. Phys. 97 (1992) 2571.
[49] P.A. Vaughan, Acta Crystallogr. 21 (1966) 983.
[50] F. Haase, J. Sauer, Micropor. Mesopor. Mater. 35–36 (2000) 379.
[51] C. Tuma, unpublished results obtained with the CPMD code.
[52] J. Sauer, P. Ugliengo, E. Garrone, V.R. Saunders, Chem. Rev. 94 (1994) 2095.
[53] F. Eder, J. Lercher, Zeolites 18 (1997) 75.
[54] F. Eder, M. Stockenhuber, J.A. Lercher, in: L. Bonneviot, S. Kaliaguine (Eds.), Zeolites: A Refined Tool for Designing Catalytic Sites, Quebec, Stud. Surf. Sci. Catal., vol. 97, Elsevier, Amsterdam, 1995, p. 495.
[55] F. Eder, J. Lercher, J. Phys. Chem. B 101 (1997) 1273.
[56] N.W. Cant, W.K. Hall, J. Catal. 25 (1972) 161.
[57] L. Benco, J. Hafner, F. Hutschka, H. Toulhoat, J. Phys. Chem. B 107 (2003) 9756.
[58] L.M. Sverdlov, M.A. Kovner, E.P. Krainov, Vibrational Spectra of Polyatomic Molecules, Wiley, New York, 1974.
[59] T. Shimanouchi, Tables of Molecular Vibrational Frequncies, vol. 1, NSRDS NBS-39, 1967.
[60] L.A. Clark, M. Sierka, J. Sauer, in: R. Aiello, G. Giordano, F. Testa (Eds.), Impact of Zeolites and other Porous Materials on the New Technologies at the Beginning of the New Millennium, 2nd FEZA Conference, Giardini Naxos, Italy, Stud. Surf. Sci. Catal., vol. 142, Elsevier, Amsterdam, 2002, p. 643.
[61] C. Tuma, J. Sauer (2005), in preparation.
[62] A. Bhan, Y.V. Joshi, N. Delgass, K.T. Thomson, J. Phys. Chem. B 107 (2003) 10476.
[63] M. Boronat, P.M. Viruela, A. Corma, J. Am. Chem. Soc. 126 (2004) 3300.
[64] L. Domokos, L. Leffers, K. Seshan, J.A. Lercher, J. Catal. 197 (2001) 68.
[65] H. Liu, G.D. Lei, W.M.H. Sachtler, Appl. Catal. A 137 (1996) 167.
[66] S. Svelle, S. Kolboe, O. Swang, J. Phys. Chem. B 108 (2004) 2953.